Electronic Supplementary Information

Ultra-small $NiFe_2O_4$ hollow particle/graphene hybrid: fabrication and electromagnetic wave absorption property

Feng Yan,[a,b,c] Dong Guo,[a] Shen Zhang,[a] Chunyan Li,*[a] Chunling Zhu,*[b] Xitian Zhang[c] and Yujin Chen*[a]

[a] Key Laboratory of In-Fiber Integrated Optics, Ministry of Education and College of Science, Harbin Engineering University, Harbin 150001, China.

[b] College of Chemistry and Chemical Engineering, Harbin Engineering University, Harbin 150001, China.

[c] Key Laboratory for Photonic and Electronic Bandgap Materials, Ministry of Education and School of Physics and Electronic Engineering, Harbin Normal University, Harbin 150025, China.

*Corresponding authors.
Tel.: +086-0451-82519754, Fax: +086-0451-82519754
E-mail addresses: chunyanli@hrbeu.edu.cn (C. Li), zhuchunling@hrbeu.edu.cn (C. Zhu) or chenyujin@hrbeu.edu.cn (Y. Chen).

Experimental details

Chemicals. Graphene sheets were purchased from Nanjing XFNANO Material Tech Co., Ltd. (Nanjing City, China). Ferric acetylacetonate, nickel acetate and ammonia were purchased from Tianjin Kermel Chemical Reagent Co., Ltd. (China). Other regents were purchased without further purification.

Synthesis of $NiFe_2O_4$-h/G composite. Graphene (24 mg) was dispersed in ethanol (72 mL), and then ferric acetylacetonate (57 mg), nickel acetate (150 mg) was added to the mixture above, respectively. After sonication for 15 min, distilled water (3.6 mL) and ammonia (2 mL) were added. The resultant mixture was kept at 80 °C for 10 h under stirring. The precipitate (NiFe hydroxide/G) was obtained by washing with distilled water and ethanol for several times and drying through a freeze-drying process. In the next step, the NiFe hydroxide/G composite was treated in a furnace at 350 °C for 3 h under an H_2/ Ar flow, then at 200 °C for 3 h and 280 °C for 3 h under air atmosphere, respectively. After cooling to room temperature, the $NiFe_2O_4$-h/G composite was obtained.

Synthesis of $NiFe_2O_4$-s/G and $NiFe_2O_4$-s composites. As a comparison, $NiFe_2O_4$-s/G was synthesized under the similar conditions except that the thermal treatment of NiFe hydroxide/G composite was carried out 200°C for 3 h and 280°C for 3 h under air atmosphere. Solid $NiFe_2O_4$ NPs were synthesized through the reported method.[1]

Structure Characterizations. XRD data were measured by a Rigaku D/max-2600/PC with Cu Kα radiation (λ=1.5418Å). The morphology and size of samples were characterized by scanning electron microscope (Hitachi SU70) and an FEI

Tecnai-F20 transmission electron microscope equipped with a Gatan imaging filter (GIF). BET surface area and pore volume were tested with a Quantachrome Instruments NOVA4000 after the composites were vacuum dried at 200℃ over 10 h. XPS analyses were carried out by using a spectrometer with Mg Kα radiation (PHI 5700 ESCA System).The binding energy was calibrated with the C 1s position of contaminant carbon in the vacuum chamber of the XPS instrument (284.6 eV). The magnetic property of the $NiFe_2O_4$ hollow particle was measured by a vibrating sample magnetometer (VSM; Lakeshore 7410) at room temperature.

The size calculation of the $NiFe_2O_4$ NPs by Scherrer equation. The crystallite sizes of the $NiFe_2O_4$ NPs with different relevant data of crystal planes are calculated by Scherrer equation:

$$D = 0.9\lambda / \beta \cos\theta$$

where D is the crystallite size， λ is the X-ray wavelength (0.15418 nm), β is the half-maximum breadth and θ is the Bragg angle of different planes.

Electromagnetic parameter Measurements. The electromagnetic parameters of the absorbers were measured by using a vector network analyzer (Anritsu MS4644A Vectorstar). The cylindrical sample (with 3.00 mm inner diameter, 7.00 mm outer diameter and 3.00 mm thickness) was prepared by mixing the absorbing materials with a paraffin matrix and the addition amount of absorbing materials into paraffin matrix paraffin matrix was controlled to be 15 wt%. Before measurement, the electromagnetic parameter was verified by standard Teflon sample with the same shape and size as the tested sample.

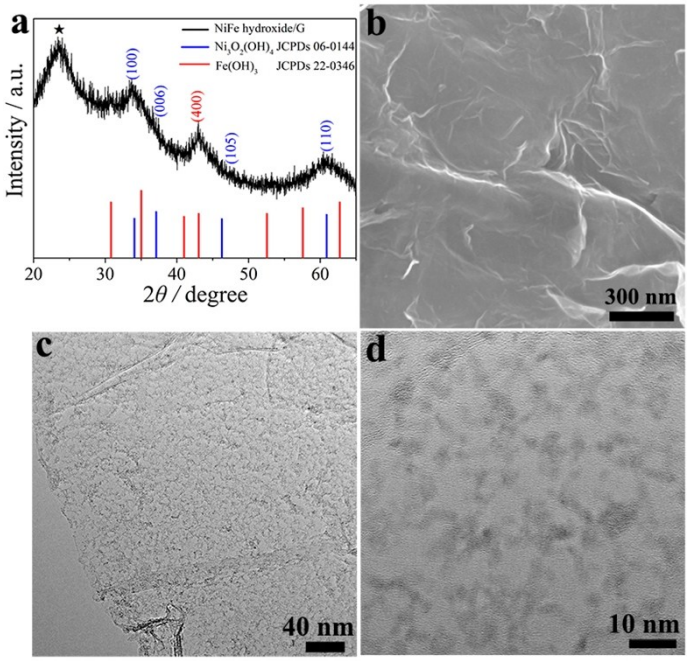

Fig. S1 (a) The XRD pattern, (b) low-magnification SEM image, (c) low-magnification image and (d) middle-magnification TEM image of NiFe hydroxide/G.

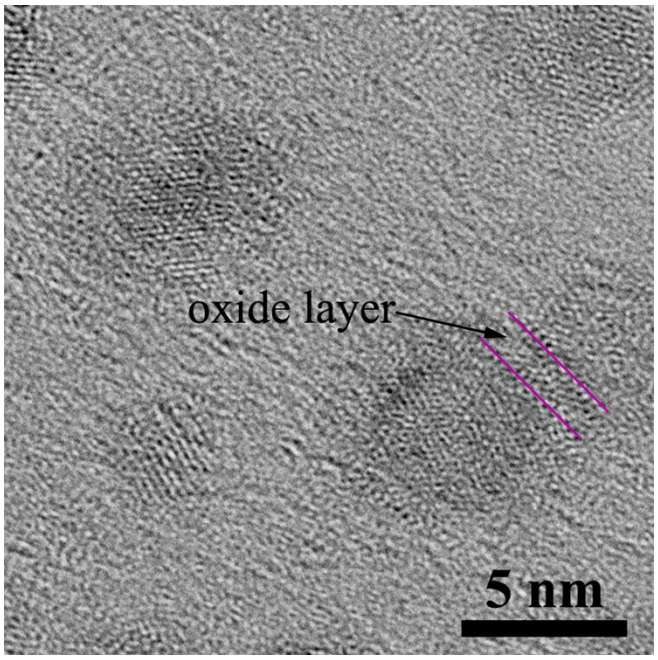

Fig. S2 The HRTEM image of NiFe/G.

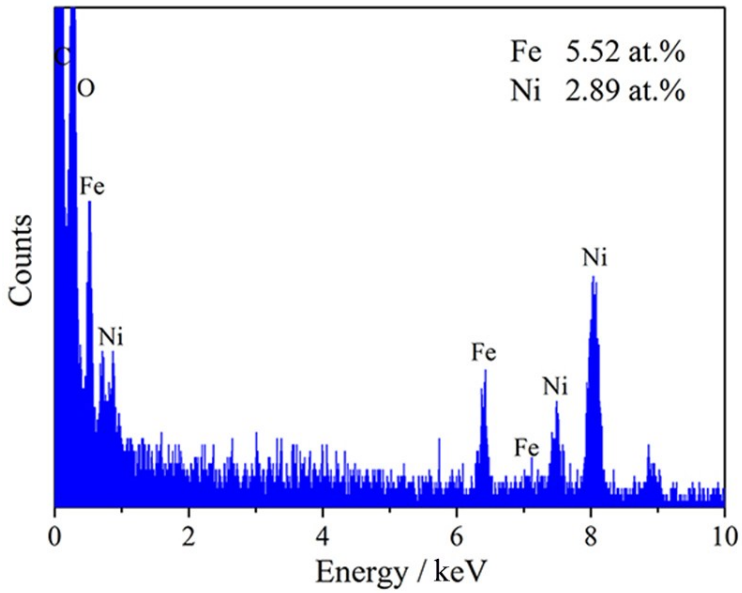

Fig. S3 The EDX pattern of $NiFe_2O_4$-h/G.

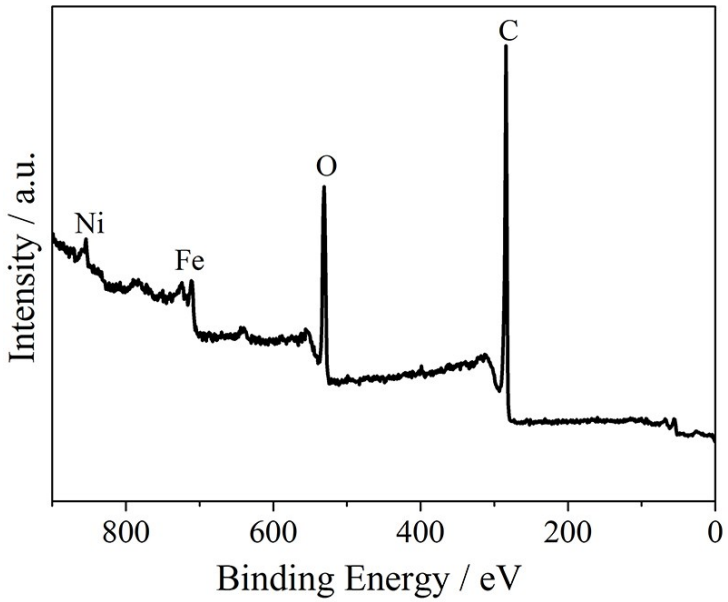

Fig. S4 The survey XPS spectrum of $NiFe_2O_4$-h/G.

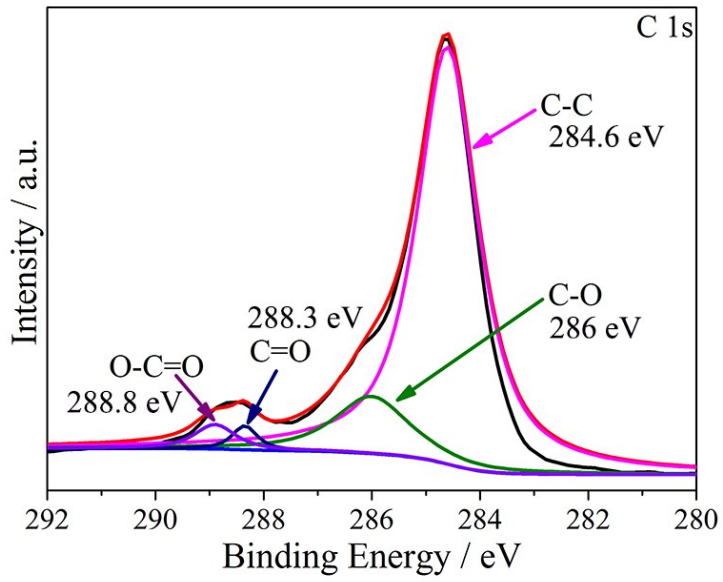

Fig. S5 The XPS spectra of C 1s core level spectrum for $NiFe_2O_4$-h/G hybrid.

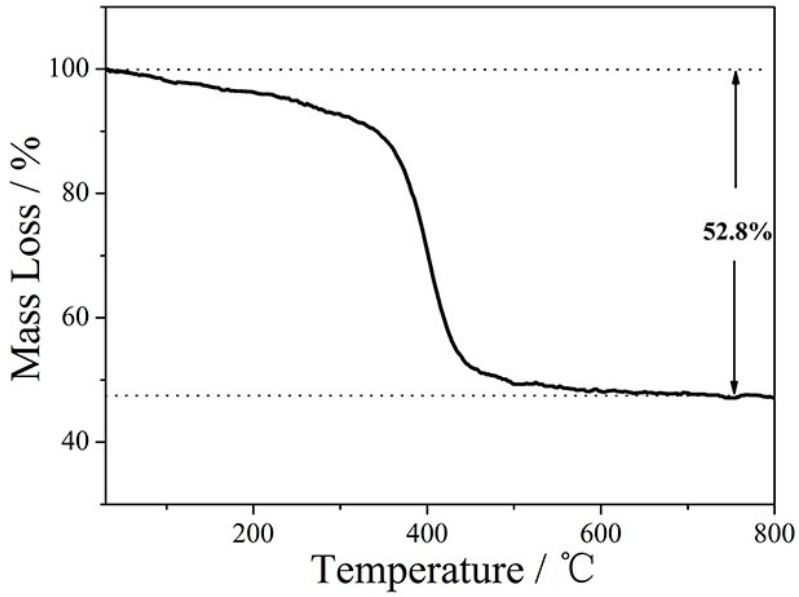

Fig. S6 The TGA analysis of $NiFe_2O_4$-h/G.

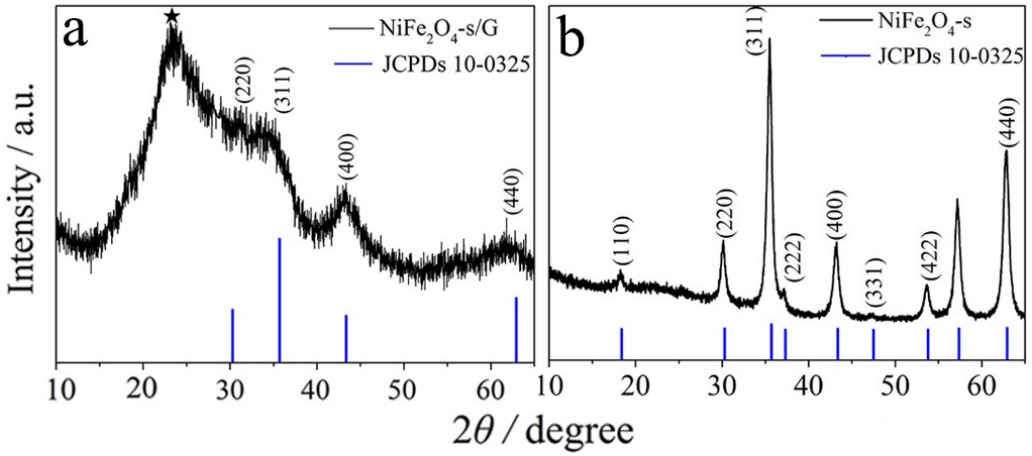

Fig. S7 The XRD patterns of (a) $NiFe_2O_4$-s/G and (b) $NiFe_2O_4$-s.

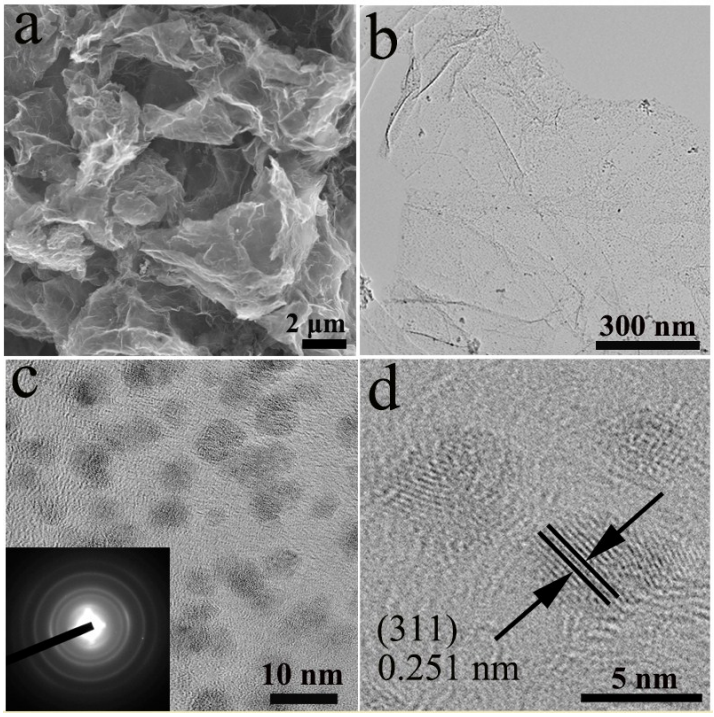

Fig. S8 (a) The Low-magnification SEM image of $NiFe_2O_4$-s/G. (b,c) TEM and (d) HRTEM images of $NiFe_2O_4$-s/G. The inset of (c) shows the corresponding SAED pattern.

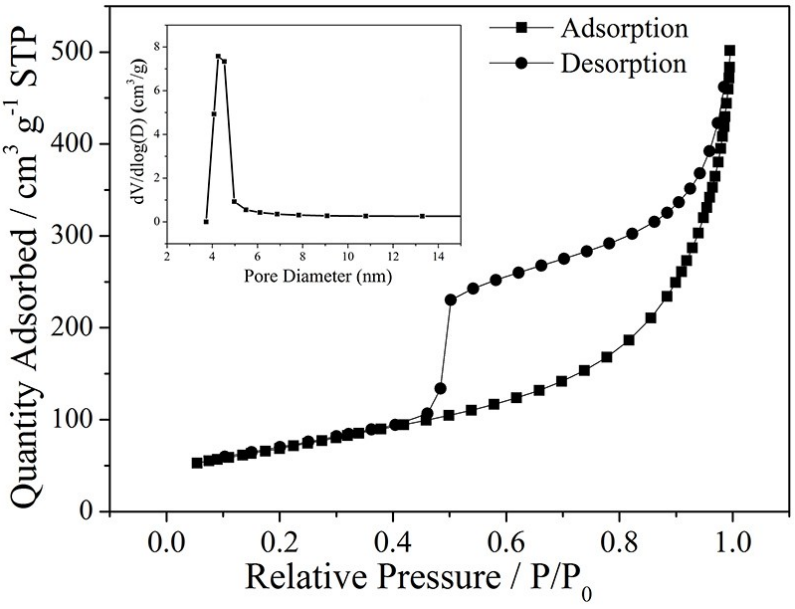

Fig. S9 Nitrogen adsorption and desorption isotherms of $NiFe_2O_4$-s/G. The inset shows the corresponding pore-size distribution calculated by the BJH method.

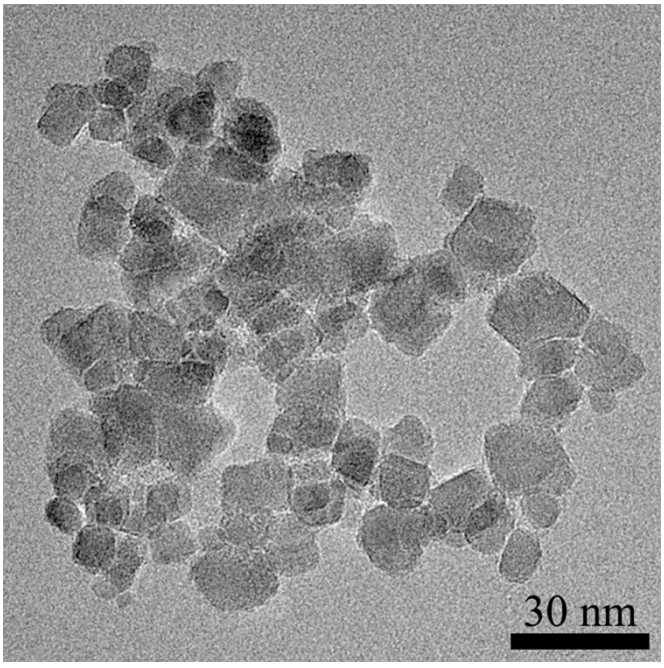

Fig. S10 The TEM image of $NiFe_2O_4$-s.

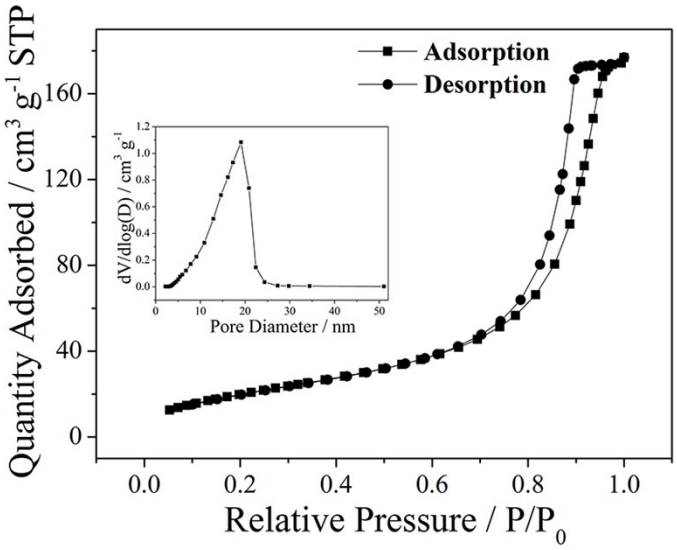

Fig. S11 Nitrogen adsorption and desorption isotherms of $NiFe_2O_4$-s. The inset shows the corresponding pore-size distribution calculated by the BJH method.

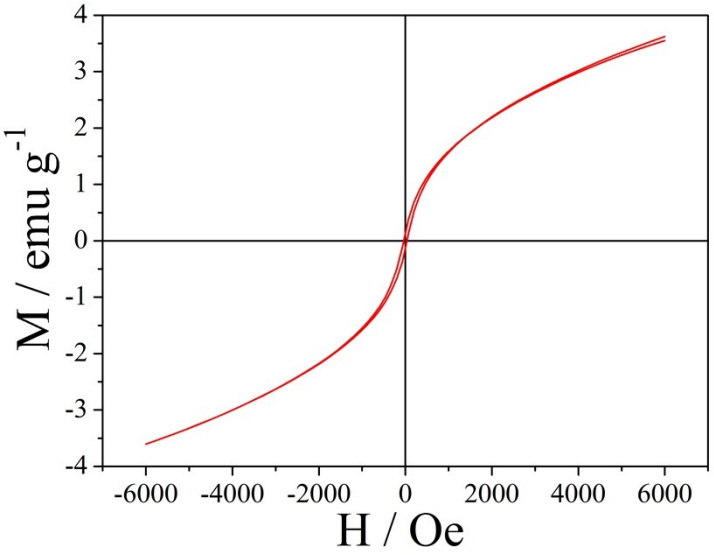

Fig. S12 Magnetization hysteresis loops of the $NiFe_2O_4$-h/G.

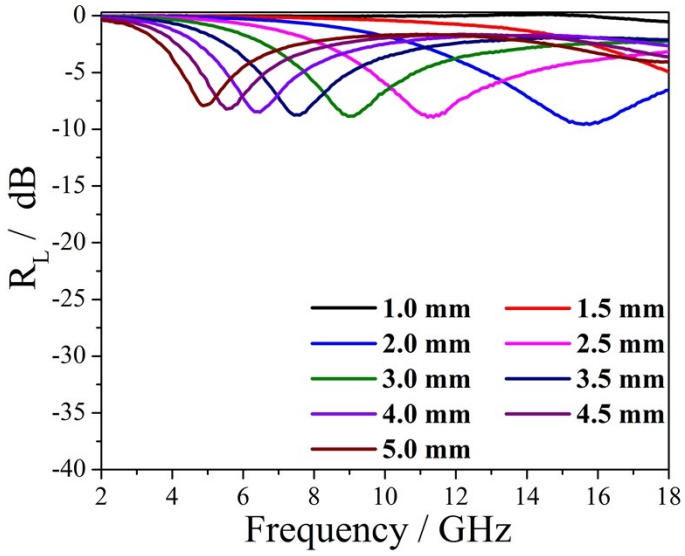

Fig. S13 The R_L–f curves of graphene sheets with different thicknesses in the frequency range of 2 – 18 GHz.

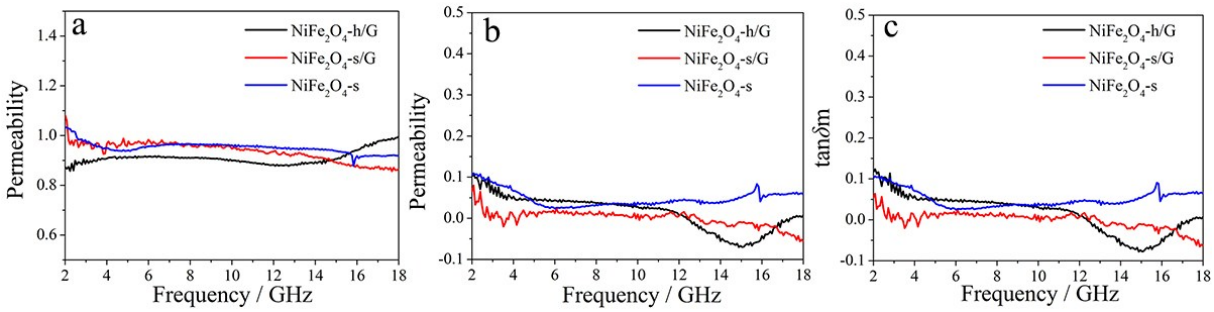

Fig. S14 (a) The real part of relative permeability, (b) imaginary part of relative permeability and (c) magnetic loss tangent of $NiFe_2O_4$-s, $NiFe_2O_4$-s/G and $NiFe_2O_4$-h/G.

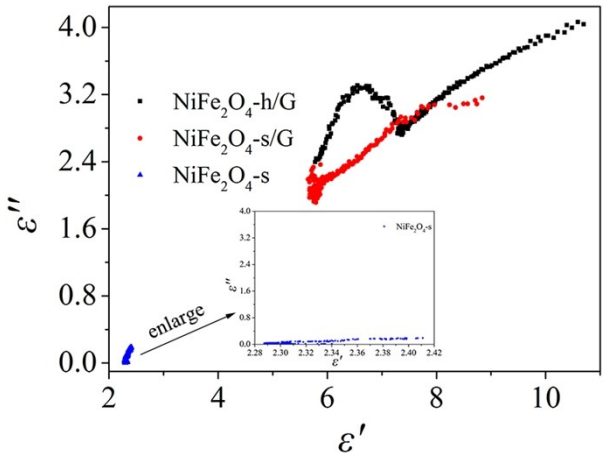

Fig. S15 The Cole-Cole semicircles of $NiFe_2O_4$-s, $NiFe_2O_4$-s/G and $NiFe_2O_4$-h/G. The inset shows the Cole-Cole semicircles of $NiFe_2O_4$-s in a high magnification resolution.

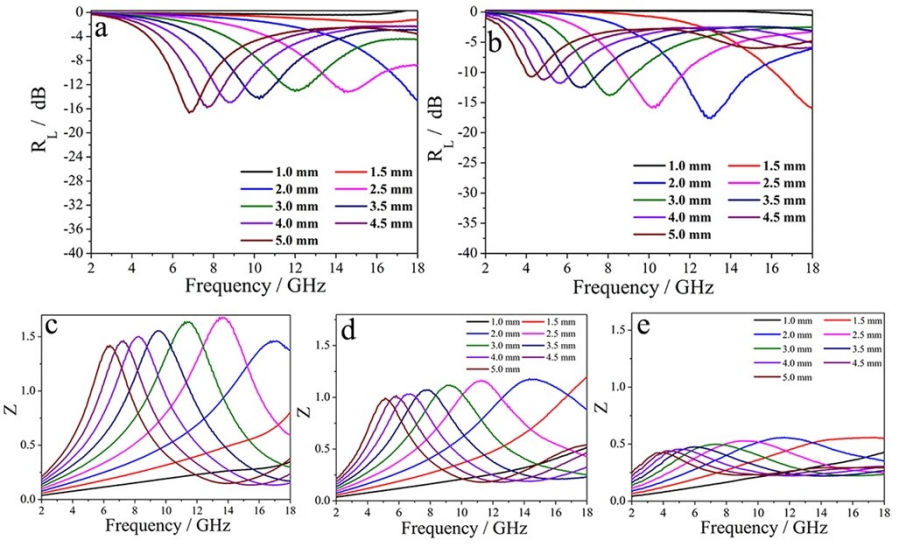

Fig. S16 (a, b) The R_L–f curves of the $NiFe_2O_4$-h/G with 10 and 20wt% of the addition amount in the frequency range of 2 – 18 GHz, respectively. (c-e) The modulus of the normalized characteristic impedance ($Z=|Z_{in}/Z_0|$) for the $NiFe_2O_4$-h/G with 10, 15 and 20 wt% of the addition amount, respectively.

Note: The R_L is highly relevant to the matched characteristic impedance. If the input impedance of an absorber matches well with the impedance of free space, most incident EMW can enter into the absorber material and then will be converted to thermal energy or dissipated through interference. Usually, the normalized characteristic impedance (Z_{in}/Z_0) can calculate from ε_r and μ_r by the following equations:

$$Z_{in} = Z_0\sqrt{\mu_r/\varepsilon_r}\tanh[j(2\pi fd/c)\sqrt{\mu_r\varepsilon_r}] \quad (1)$$

when Z (the modulus of the normalized characteristic impedance, $Z = |Z_{in}/Z_0|$) is equal or close to 1, the absorber will possess good impedance matching characteristic. As shown in S16c-e, the values for the $NiFe_2O_4$-h/G with 15 wt% of the addition amount are more near to 1 at d ranging from 3.5 to 5.0 mm than those for the $NiFe_2O_4$-h/G with 10 wt% of the addition amount and for the $NiFe_2O_4$-h/G with 20 wt% of the addition amount, indicating the best impedance matching property of the $NiFe_2O_4$-h/G with 15 wt% of the addition amount among these composites.

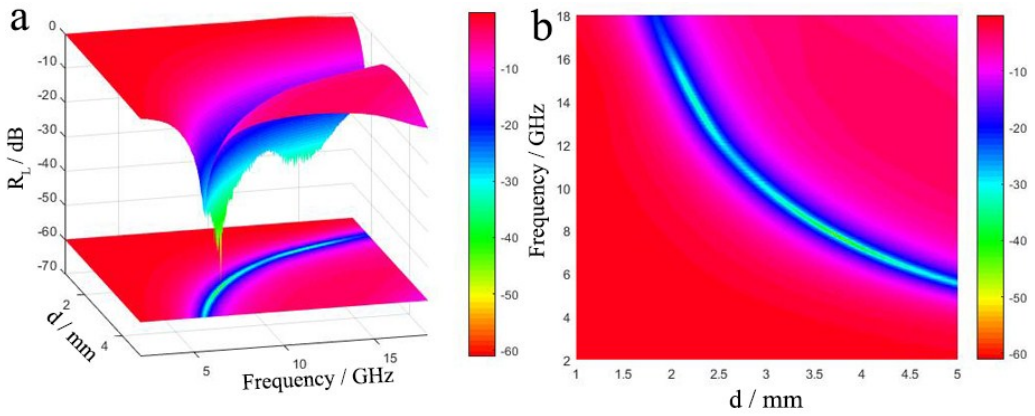

Fig. S17 Three-dimensional representation of R_L values for $NiFe_2O_4$-h/G with different thicknesses in the frequency range of 2 – 18 GHz.

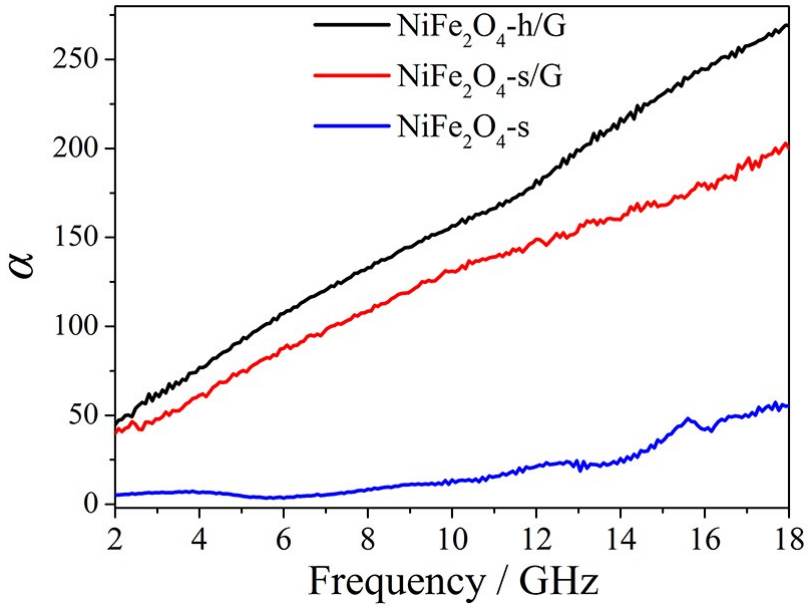

Fig. S18 The attenuation constants of $NiFe_2O_4$-s, $NiFe_2O_4$-s/G and $NiFe_2O_4$-h/G in the frequency range of 2 – 18 GHz.

Table S1. The crystallite sizes of the $NiFe_2O_4$ NPs calculated in terms of different relevant data of lattice planes.

crystal planes	cosθ	β	D
(311)	0.952	7.981°	~1.0 nm
(400)	0.929	3.528°	~2.4 nm
(440)	0.853	3.123°	~3.0 nm

Table S2. Comparison of the efficient absorption widths between $NiFe_2O_4$-h/G and $NiFe_2O_4$-s/G at different thickness.

d (mm) / EBWs (GHz)	2.5	3	3.5	4	4.5	5
$NiFe_2O_4$-h/G	4.5	3.3	2.8	2.4	1.3	1.8
$NiFe_2O_4$-S/G	3.9	3.4	3.0	2.7	2.4	2.0

Table S3. Comparison of EMW absorption properties of $NiFe_2O_4$-h/G with those of other absorbing materials.

Materials	Minimal R_L (dB)	*d* (mm)	EBW (GHz)	C (wt %)	Ref.
RGO/$NiFe_2O_4$	-39.7	3.0	~3.0	50	[2]
$NiFe_2O_4$ nanorod–graphene	-44.6	4.0	~2.6	60	[3]
$NiFe_2O_4$ nanoparticle–graphene	-27.9	4.0	~2.7	60	
$NiFe_2O_4$-polystyrene	-13.0	2.0	2.7	65	[4]
$CoFe_2O_4$/graphene	-24.7	4.0	~2.4	60	[5]
graphene–Fe_3O_4/ZnO	-40.0	5.0	~1.7	30	[6]
FeCo/graphene	-40.2	2.5	~4.1	50	[7]
$Co_{20}Ni_{80}$	-33.5	5.0	~1.8	-	[8]
Co_3O_4/RGO	-32.3	2.5	~5.2	20	[9]
Ni fiber	-39.5	3.0	~1.1	50	[10]
Porous Co/C	-35.3	4.0	~2.4	40	[11]
Graphene/Fe_3O_4@Fe/ZnO	-38.4	5.0	~2.9	20	[12]
Fe_3O_4/GCs	-32.0	3.5	~4.8	30	[13]
$NiFe_2O_4$-s/G	-20.2	5.0	2.1	15	This work
$NiFe_2O_4$-h/G	-40.9	3.5	2.8	15	This work

REFERENCES

1. P. B. Liu, Y. Huang and X. Zhang, *Composites Science and Technology* 2014, **95**, 107.
2. M. Zong, Y. Huang, X. Ding, N. Zhang, C. H. Qu and Y. L. Wang, *Ceramics International* 2014, **40**, 6821.
3. M. Fu, Q. Z. Jiao and Yun. Zhao, *J. Mater. Chem. A* 2013, **1**, 5577.
4. H. T. Zhao, X. D. Sun, C. H. Mao and J. Du, *Physica B* 2009, **404**, 69.
5. M. Fu, Q. Z. Jiao, Y. Zhao and H. S. Li, *J. Mater. Chem. A* 2014, **2**, 735.
6. D. P. Sun, Q. Zou, Y. P. Wang, Y. J. Wang, W. Jiang and F. S. Li, *Nanoscale* 2014, **6**, 6557.
7. X. H. Li, J. Feng, Y. P. Du, J. T. Bai, H. M. Fan, H. L. Zhang, Y. Peng and F. S. Li, *J. Mater. Chem. A*, 2015, **3**, 5535.
8. Q. H. Liu, X. H. Xu, W. X. Xia, R. C. Che, C. Chen, Q Cao and J. G. He, *Nanoscale* 2015, **7**, 1736.
9. X. B. Li, S. W. Yang, J. Sun, P. He, X. P. Pu and G. Q. Ding, *Synthetic Metals* 2014, **194**, 52.
10. C. H. Gong, J. W. Zhang, X. F. Zhang, L. G. Yu, P. Y. Zhang, Z. S. Wu and Z. J. Zhang, *J. Phys. Chem. C* 2010, **114***,* 10101.
11. Y. Y. Lü, Y. T. Wang, H. L. Li, Y. Lin, Z. Y. Jiang, Z. X. Xie, Q. Kuang and L. S. Zheng, *ACS Appl. Mater. Interfaces* 2015, **7**, 13604.
12. Y. L. Ren, H. Y. Wu, M. M. Lu, Y. J. Chen, C. L. Zhu, P. Gao, M. S. Cao, C. Y. Li and Q. Y. Ouyang, *ACS Appl. Mater. Interfaces* 2012, **4**, 6436.

13. X. Jian, B. Wu, Y. F. Wei, S. X. Dou, X. L. Wang, W. D. He and N. Mahmood, *ACS Appl. Mater. Interfaces* 2016, **8**, 6101.